Impact of Pore Connectivity on the Design of Long-Lived Zeolite Catalysts

Originally published in:
Angewandte Chemie. International Edition 54(5), https://doi.org/10.1002/anie.201410016

Funding acknowledgement:
134572 - A fundamental approach to the scale up of hierarchical zeolite catalysts (SNF)
132059 - Testing antigravity with positronium (SNF)

Impact of Pore Connectivity in the Design of Long-Lived Zeolite Catalysts**

Maria Milina, Sharon Mitchell, David Cooke, Paolo Crivelli, and Javier Pérez-Ramírez*

Abstract: *Without sensitive techniques to complex pore architectures, synthetic efforts to enhance molecular transport in zeolite and other porous materials through hierarchical structuring, lack descriptors for their rational design. Here, we demonstrate the power of positron annihilation lifetime spectroscopy (PALS) to characterize the pore connectivity in hierarchical MFI zeolites, establishing a direct link with the enhanced catalyst lifetime in the conversion of methanol to valuable hydrocarbons. The unique ability to capture subtleties of the hierarchical structure originates from the dynamic nature of the ortho-positronium response to the pore network. The findings reveal the strong dependence on the way in which the hierarchical zeolites are manufactured, having direct implications for the practical realization of these advanced catalysts.*

Complex porous materials are pivotal in the development of many cutting-edge technologies, the pore network typically balancing the efficiency of a physical process with specific chemical functions.[1] Hierarchically-structured zeolite catalysts are an elegant example of systems in which the introduction of an auxiliary network of meso- and/or macropores to facilitate molecular transport to the active sites located in the micropores yields enhanced performance in numerous hydrocarbon transformations.[2] To optimize the design of such materials, it is imperative to correlate the pore topology, determined by the amount, size, connectivity, and distribution of each porosity level, with the catalytic impact. This requires both sensitive techniques to relevant pore characteristics and the availability of materials with comparable bulk properties, but differing pore topology. One of the most powerful methods to assess the pore structure is undoubtedly the direct visualization by transmission electron tomography, which has enabled the derivation of the tortuosity and accessibility of mesopores within individual zeolite crystals.[3] Over a wider range of length scales, such as those spanned in technical zeolite bodies, integrated imaging approaches coupled with dedicated sample preparation become necessary.[4] Indirect methods, such as hyperpolarized ^{129}Xe or pulsed field gradient (PFG-) NMR, have also attracted interest to study the interconnectivity of the micro- and mesopores.[5] However, to date none of the parameters derived have been quantitatively correlated with the catalytic performance.

By introducing a top-down demetallation strategy to develop distinct 'open' or 'constricted' mesopore configurations in MFI-type crystals, we recently exposed the major impact of pore architecture on the lifetime of the hierarchical zeolites in the conversion of methanol to hydrocarbons (MTH).[6] The dissimilar pore structures of these model catalysts could be readily distinguished from the relative mesopore volume determined by gas sorption and mercury porosimetry, identical-location scanning transmission and secondary electron microscopy, and positron annihilation lifetime spectroscopy (PALS). Yet, to really push the performance and economic boundaries of zeolite catalysts, a much more precise understanding of the role of the hierarchical pore network is required in relevant platforms of materials. Here, taking desilication as a highly scalable and versatile manufacturing method,[7] we have followed different approaches altering the concentration (x = 0.05-0.3 M NaOH) and duration (y = 5-30 min) of alkaline treatment to prepare a matrix of hierarchical zeolites (ATx-y) of widely differing mesoporosity, depending on the extent of dissolution (Table 1). Comparatively, as shown in the same table, the acidic properties of the samples vary within a very narrow range.

Evaluation of the hierarchical zeolites in the MTH reaction (Figure 1) confirms large differences in the cycle time, defined as the time for which the conversion exceeds 95%, which is extended by between 1.3-3.6 times that of the conventional analogue (C). Only minor variations in the average product selectivity to light olefins ($S_{C2\text{-}C4\ olefins}$ = 40±2 Cmol%) or aromatics ($S_{C6\text{-}C8\ aromatics}$ = 12±4 Cmol%) were evidenced over the catalysts under the conditions studied (Table S1). The similar product distribution is consistent with the comparable active-site quality, indicating that the lifetime differences derive from the quality of the pore structure. While some cycle times,

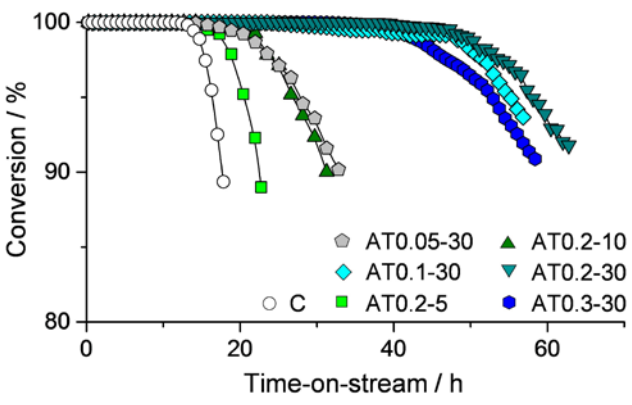

Figure 1. Conversion versus time-on-stream in the MTH reaction over the zeolites (T = 723 K, P = 1 bar, $WHSV$ = 9.5 $g_{methanol}$ $g_{zeolite}^{-1}$ h^{-1}).

[*] M. Milina, Dr. S. Mitchell, Prof. J. Pérez-Ramírez
ETH Zurich, Department of Chemistry and Applied Biosciences
Institute for Chemical and Bioengineering
Vladimir-Prelog-Weg 1, 8093 Zurich
E-mail: jpr@chem.ethz.ch

Dr. D. Cooke, Dr. P. Crivelli
ETH Zurich, Department of Physics
Institute for Particle Physics
Otto-Stern-Weg 5, 8093 Zurich

[**] This work was supported by the Swiss National Science Foundation (Project: 200021-134572 and Ambizione grant PZ00P2-132059) and ETH Zurich (Grant ETH-47-12-1)

Supporting information for this article is given via a link at the end of the document.

Table 1. Composition, bulk porous and acidic properties, and pore connectivity of the ZSM-5 zeolites.

Sample	Si/Al mol mol^{-1}	V_{micro}[a] cm^3 g^{-1}	$V_{meso,N2}$[b] cm^3 g^{-1}	$V_{meso,Hg}$[c] cm^3 g^{-1}	S_{meso}[a] m^2 g^{-1}	d_{meso}[d] nm	$c_{Brønsted}$[e] µmol g^{-1}	c_{Lewis}[e] µmol g^{-1}	C_{pore}[f] -
C	40	0.17	0.11	0.05	78	-	174	19	0.34
AT0.05-30	38	0.16	0.14	0.05	98	-	175	32	0.65
AT0.1-30	35	0.15	0.19	0.10	135	6	151	39	0.78
AT0.2-5	34	0.15	0.22	0.06	139	<4	150	49	0.45
AT0.2-10	30	0.14	0.30	0.10	205	5	145	52	0.56
AT0.2-30	25	0.12	0.39	0.25	272	8	147	78	0.83
AT0.3-30	21	0.09	0.72	0.49	376	13	146	75	0.80

[a] *t*-plot method; [b] $V_{meso,N2} = V_{total}-V_{micro}$; [c] volume of Hg intruded in mesopores of 3.8-50 nm in diameter; [d] average mesopore diameter from the BJH method; [e] IR study of adsorbed pyridine; [f] $C_{pore} = Ps_{vacuum}/Ps_{total}$ determined by PALS.

such as the behavior of the samples alkaline treated for different times at fixed concentration (AT0.2-5 < AT0.2-10 < AT0.2-30), appear to simply relate to the increasing degree of mesoporosity, evidenced by N_2 sorption, Hg intrusion, and transmission electron microscopy (Table 1, Figures S1 and S2), others are less straightforward to explain. In particular, the equivalent lifetime extensions (ca. 3.5 times that of C) displayed by zeolites treated for a fixed time at different concentrations (AT0.1-30 ≈ AT0.2-30 ≈ AT0.3-30) appear to be independent of the widely varying mesoporosity. This indicates that despite being sensitive to differences in the pore structure the bulk textural parameters derived by these techniques are not suitable descriptors and has huge implications for the manufacturing efficiency of hierarchical zeolites as the amount of mesopores introduced directly relates to the yield of alkaline treatment (Figure S3). A second striking observation is the huge difference in the performance of the zeolites prepared with shorter stronger or longer milder treatments (AT0.2-05 and AT0.1-30). Aside from a slightly smaller average mesopore size in the former (Figure S2), these samples exhibit negligible differences in bulk porosity, suggesting that standard techniques are insensitive to subtleties in the pore structure which can appreciably impact the lifetime.

Clearly there is a need for better methods to optimize the design of zeolite catalysts. The recent addition of PALS to the characterization toolbox of hierarchical zeolites could contribute to the improved understanding of the pore topology.[6] In particular, the dynamic response of the annihilation of ortho-positronium (*o*-Ps) species formed upon positron implantation into the sample contains information about the pore connectivity.[8] If the pores are accessible to the external surface, *o*-Ps species can escape into vacuum, decaying with a characteristic lifetime of 142 ns. Otherwise, they may become entrapped within the material where, due to the increased probability of surface collisions, the lifetime reduces with decreasing pore size. Thus, the fraction of the total amount of *o*-Ps formed which is emitted into vacuum offers a direct measure of the *global pore connectivity* ($C_{pore} = Ps_{vacuum}/Ps_{total}$) in the hierarchical zeolites (Tables 1 and S2). Remarkably, this parameter is found to excellently describe the MTH lifetime of all of the zeolites (Figure 2), including that of the previously reported system with constricted mesopores (AT0.2-TPA-30).[6]

The equivalent global connectivity determined by PALS and the plateauing dependence of the MTH lifetime with the mesopore volume and yield of zeolites prepared with different NaOH concentrations at longer treatment times (Figures 3a,b), point toward a critical mesopore size above which further enlargement no longer benefits the removal of coke precursors during the reaction. Analysis of the porosity of the catalysts at the end of the cycle (Table S3) corroborates this hypothesis; the higher mesopore volume retained in the spent AT0.3-30 zeolite compared to AT0.1-30, indicating that this zeolite is excessively dissolved as the additional porosity does not contribute to an improved coke tolerance. On the other hand, the distinct pore connectivity and performance of zeolites of equivalent mesoporosity (AT0.2-5 and AT0.1-30) prepared with shorter concentrated or longer mild treatments are tentatively ascribed to differences in the mechanism of mesopore formation. Under the former conditions, the smaller nascent mesopores develop most prominently along grain boundaries of the zeolite crystals which appear comparatively pristine (Figures 3c and S4). In contrast, prolonged treatments appear to favor the more directed development of larger interconnected and intracrystalline

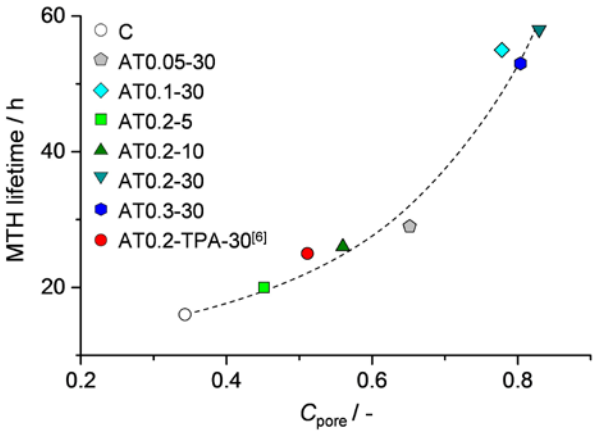

Figure 2. Correlation between the MTH lifetime of the zeolites and the global pore connectivity.

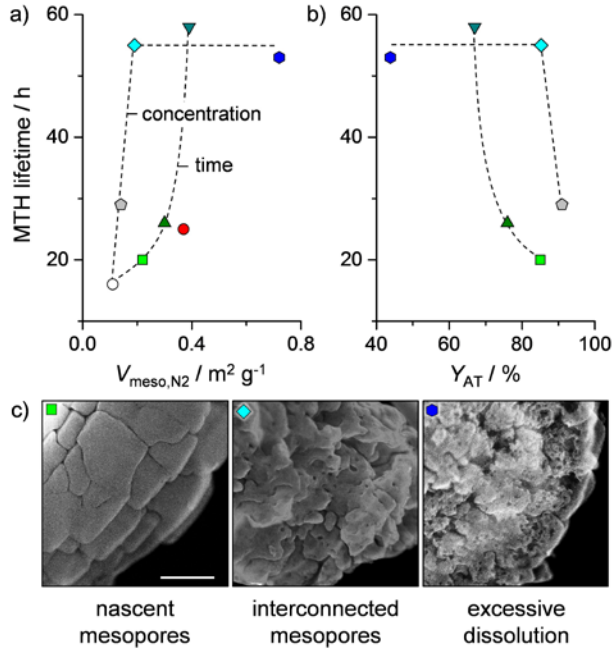

Figure 3. Correlation between the MTH catalyst lifetime and a) the mesopore volume and b) the yield of alkaline treatment. c) Scanning electron micrographs expose the distinct mesopore structure of hierarchical zeolites prepared by alkaline treatment for different time or concentration. See Figure 2 for legend. In part c, the scale bar represents 100 nm and applies to all images.

mesopores, which enhance the active site accessibility. Distinct modes of mesopore formation by desilication have been previously postulated to originate from differences in the zeolite composition and particle morphology,[9] but our results show that the treatment conditions also have a strong impact.

In summary, this contribution has demonstrated the unprecedented sensitivity of PALS to the impact of subtle differences in the pore structure which govern the tolerance of hierarchical zeolites to coking in hydrocarbon transformations. This exceptional ability can be attributed to the extremely short temporal probing window of positronium to the pore network compared with most other techniques of porosity assessment. Advantageously, the pore connectivity derived requires no parameterization and thus, unlike other common porosity variables, is not influenced by prior assumptions about the geometry, surface interactions, etc. Furthermore, the technique is not limited to the analysis of powders; the equivalent global connectivity evidenced for AT0.2-30 following extrusion with a kaolin binder confirmed that the interaction between the component phases did not hinder the escape of o-Ps due to pore blockage (Table S1). However, as the lifetime of *o*-Ps in large pores (e.g. > 100 nm in diameter) becomes comparable to the value in vacuum, the connectivity of the macropore network in shaped bodies cannot be directly extracted from the PALS spectra. In this case, the amount of *o*-Ps decaying within large interparticle voids could be determined by the simultaneous application of a time-of-flight (TOF) detector. Thus, the application of PALS, which is currently unexplored in catalysis, opens new doors for the improved design of diverse porous materials over a wide range of length scales.

Experimental Section

Alkaline treatments of the conventional ZSM-5 zeolite (CBV 8014, Zeolyst International) were performed in stirred 0.05-0.3 M NaOH solutions (30 $cm^3\ g_{zeolite}^{-1}$) at 338 K for 5-30 min. All samples were converted into protonic form by three consecutive ion exchanges in an aqueous NH_4NO_3 solution (0.1 M, 298 K, 8 h, 100 $cm^3\ g_{zeolite}^{-1}$) and calcined at 823 K (5 K min^{-1}) for 5 h prior to characterization and catalytic evaluation. Extrudates (4 mm diameter) were obtained by shaping AT0.2-30 zeolite with a kaolin binder (20 wt.%) followed by drying and calcination at 873 K for 5 h (5 K min^{-1}). The catalysts were characterized by inductively coupled plasma optical emission spectroscopy, nitrogen sorption, Fourier transform infrared spectroscopy of adsorbed pyridine, transmission and scanning electron microscopy, and positron annihilation lifetime spectroscopy. The methanol-to-hydrocarbons reaction was carried out in a fixed-bed reactor at 723 K and *WHSV* = 9.5 $g_{methanol}\ g_{zeolite}^{-1}\ h^{-1}$ coupled with online GC analysis. Characterization and testing procedures are fully detailed in the Supporting Information.

Keywords: heterogeneous catalysis • zeolites • pore connectivity • positron annihilation lifetime spectroscopy • methanol-to-hydrocarbons

[1] a) V. Karageorgiou, D. Kaplan, *Biomaterials* **2005**, *26*, 5474-5491; b) D. M. D'Alessandro, B. Smit, J. R. Long, *Angew. Chem. Int. Ed.* **2010**, *49*, 6058-6082; c) X. Zhao, J. Kim, C. A. Cezar, N. Huebsch, K. Leeb, K. Bouhadird, D. J. Mooney, *Proc. Nat. Acad. Sci.* **2011**, *108*, 67-72; d) N. Tétreault, M. Grätzel, *Energy Environ. Sci.* **2012**, *5*, 8506-8516; e) S. Dutta, A. Bhaumik, K. C.-W. Wu, *Energy Environ. Sci.* **2014**, doi:10.1039/c4ee01075b.

[2] a) M. Hartmann, *Angew. Chem. Int. Ed.* **2004**, *43*, 5880-5882; b) L. Tosheva, V. P. Valtchev, *Chem. Mater.* **2005**, *17*, 2494-2513; c) M. Choi, H. S. Cho, R. Srivastava, C. Venkatesan, D.-H. Choi, R. Ryoo, *Nat. Mater.* **2006**, *5*, 718-723; d) J. Pérez-Ramírez, C. H. Christensen, K. Egeblad, C. H. Christensen, J. C. Groen, *Chem. Soc. Rev.* **2008**, *37*, 2530-2542; e) S. Lopez-Orozco, A. Inayat, A. Schwab, T. Selvam, W. Schwieger, *Adv. Mater.* **2011**, *23*, 2602-2615; f) K. Na, C. Jo, J. Kim, K. Cho, J. Jung, Y. Seo, R. J. Messinger, B. F. Chmelka, R. Ryoo, *Science*, **2011**, *333*, 328-332; g) W. J. Roth, O. V. Shvets, M. Shamzhy, P. Chlubná, M. Kubů, P. Nachtigall, J. Čejka, *J. Am. Chem. Soc.* **2011**, *133*, 6130–6133; h) D. P. Serrano, J. M. Escola, P. Pizarro, *Chem. Soc. Rev.* **2013**, *42*, 4004-4035; i) W. J. Roth, P. Nachtigall, R. E. Morris, J. Čejka, *Chem. Rev.* **2014**, *114*, 4807-4837; j) Wheatly et al., *Angew. Chem. Int. Ed.* **2014**, doi:10.1002/anie.201407676.

[3] a) J. Zečević, C. J. Gommes, H. Friedrich, P. E. de Jongh, K. P. de Jong, *Angew. Chem. Int. Ed.* **2012**, *51*, 4213-4217; b) J. M. Thomas, R. K. Leary, *Angew. Chem. Int. Ed.* **2014**, *53*, 2-4.

[4] a) S. Mitchell, N.-L. Michels, K. Kunze, J. Pérez-Ramírez, *Nat. Chem.* **2012**, *4*, 825-831; b) B. M. Weckhuysen, *Angew. Chem. Int. Ed.* **2009**, *48*, 4910-4943.

[5] a) K. Cho, H. S. Cho, L.-C. Menorval, R. Ryoo, *Chem. Mater.* **2009**, *21*, 5664-5673; b) J. Kärger, R. Valiullin, *Chem. Soc. Rev.* **2013**, *42*, 4172-4197; c) Q. Wang et al., *RSC Adv.* **2014**, *4*, 21479-21491.

[6] M. Milina, S. Mitchell, P. Crivelli, D. Cooke, J. Pérez-Ramírez, *Nat. Commun.* **2014**, *5:3922*, doi:10.1038/ncomms4922.

[7] J. Pérez-Ramírez, S. Mitchell, D. Verboekend, M. Milina, N.-L. Michels, F. Krumeich, N. Marti, M. Erdmann, *ChemCatChem* **2011**, *3*, 1731-1734.

[8] a) D. W. Gidley, H. G. Peng, R. S. Vallery, *Ann. Rev. Mat. Res.* **2006**, *36*, 49-79; b) D. W. Gidley, W. E. Frieze, T. L. Dull, A. F. Yee, E. T. Ryan, H.-M. Ho, *Phys. Rev. B* **1999**, *60*, 5157-5160.

[9] S. Svelle, L. Sommer, K. Barbera, P.N.R. Vennestrøm, U. Olsbye, K. P. Lillerud, S. Bordiga, Y.-H. Pan, P. Beato, *Catal. Today* **2011**, *168*, 38-47.

Entry for the Table of Contents

COMMUNICATION

Well connected? The sensitivity of positron annihilation lifetime spectroscopy (PALS) to subtleties in the pore connectivity of hierarchical zeolite catalysts arising from variations in the synthesis protocol, enables rationalization of their distinct lifetime in the conversion of methanol to hydrocarbons (MTH). The findings have huge implications for the manufacturing efficiency and performance of these and other advanced porous materials.

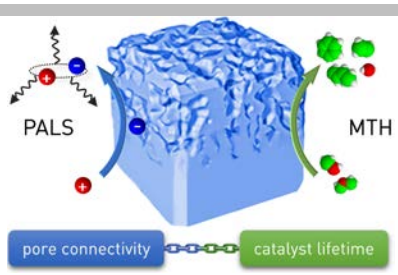

*Maria Milina, Sharon Mitchell, David Cooke, Paolo Crivelli, Javier Pérez-Ramírez**

Page No. – Page No.

Impact of Pore Connectivity in the Design of Long-Lived Zeolite Catalysts

Catalyst characterization

The amounts of Si and Al in the solids were determined by inductively coupled plasma optical emission spectroscopy (ICP-OES) using a Horiba Ultima 2 instrument equipped with photomultiplier tube detection. Samples were dissolved in a NaOH matrix, diluted with deionized water, and measured with a 5-point calibration curve.

N_2 isotherms at 77 K were measured in a Micromeritics TriStar II instrument. The samples were evacuated at 573 K for 12 h prior to measurement. The *t*-plot method was used to estimate the micropore volume and the mesopore (external) surface area. The mesopore volume was estimated by subtraction of the micropore volume from the pore volume determined from the total amount of nitrogen adsorbed at p/p_0 = 0.98. The mesopore size distribution was obtained by the Barrett-Joyner-Halenda model applied to the adsorption branch of the isotherm.

Mercury intrusion porosimetry was undertaken with a Micromeritics Autopore IV 9510 following in situ sample evacuation and using a contact angle of 140°. The mesopore volume was determined from the amount of mercury intruded into pores of 3.8-50 nm.

Fourier transform infrared spectroscopy (FTIR) of adsorbed pyridine was undertaken using a Bruker IFS 66 spectrometer. Self-supporting zeolite wafers (1 mm^2) were degassed at 10^{-3} mbar and 693 K for 4 h prior to analysis. Following adsorption at room temperature, weakly bound pyridine molecules were evacuated at 473 K for 30 min. The concentrations of Brønsted ($c_{Brønsted}$) and Lewis (c_{Lewis}) acid sites were determined using extinction coefficients of ε(Brønsted)=1.67 cm^{-1} μmol^{-1} and ε(Lewis)=2.94 cm^{-1} μmol^{-1}.

Transmission electron micrographs were acquired using a Philips Tecnai F30 microscope operated at 300 kV. Scanning electron microscopy was performed on an aberration-corrected Hitachi HD2700C operated at 200 kV and equipped with a secondary electron detector.

Positron annihilation lifetime spectroscopy (PALS) was undertaken using the ETHZ slow positron beam.[1] The powdered zeolites were degassed in situ under vacuum at 295 K for 2 h. Monoenergetic positrons derived from a ^{22}Na source coupled to a rare-gas solid moderator were accelerated into the sample under low-energy conditions (10 keV), resulting in a mean implantation depth of 1000 nm.[2] The start signal was produced by the detection, on a microchannel plate (MCP) detector, of secondary electrons released from the target by positron impact. Annihilation photons were captured by large solid angle bismuth germanium oxide (BGO) detectors and a smaller barium fluoride (BaF_2) detector, providing the stop signals and enabling a lifetime spectrum to be built up. The combination of the BGO and BaF_2 detectors permits an increased resolution for the detection of the vacuum and short-lived components, respectively. The PALS spectra were best fitted by six exponential lifetime components. Their relative fractions were extracted using a fitting method based on Markov chain Monte-Carlo Bayesian inference calculations in the PAScual data suite[3] after subtraction of the background due to accidentals, that is, uncorrelated start-stop signals, and are fully detailed in Table S1.

Catalyst testing

The methanol-to-hydrocarbons (MTH) reaction was studied in a Microactivity Reference unit (PID Eng & Tech) using a continuous flow fixed-bed reactor (13.5 mm i.d.) at ambient pressure and 723 K. The zeolites (0.5 g, particles of 0.2-0.4 mm, diluted with 1.5 g silicon carbide, particles of 0.4-0.6 mm) were pretreated under a N_2 flow at 723 K for 30 min. Liquid methanol (99.9%) was fed into the preheating zone of the reactor using an HPLC pump (307, Gilson), where it was subsequently vaporized in a nitrogen flow (48.9 cm^3 min^{-1}) to achieve a weight hourly space velocity of 9.5 $g_{methanol}$ $g_{zeolite}^{-1}$ h^{-1}. The gaseous products were analyzed using an on-line Agilent 7890A gas chromatography equipped with an HP-PLOT Q capillary column and a flame ionization detector (FID). Both methanol and dimethylether were considered as reactant species in calculating the conversion.

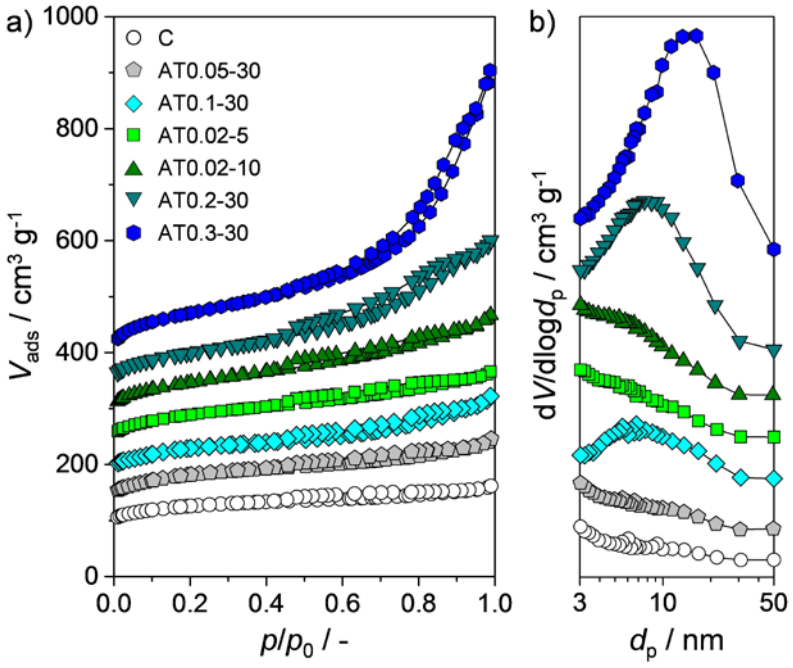

Figure S1. a) Nitrogen isotherms at 77 K and b) the Barrett-Joyner-Halenda (BJH) mesopore size distributions of the conventional (C) and hierarchical (AT*x*-*y*) ZSM-5 zeolites. In the sample code, *x* and *y* indicate the NaOH concentration (M) and length (min) of the alkaline treatment, respectively. For ease of comparison, the isotherms are vertically offset by 50 cm^3 g^{-1}.

Figure S2. (overleaf) Transmission electron micrographs of selected zeolites. While the increasing degree of mesoporosity is clearly visible in samples treated for a fixed time at higher NaOH concentration (AT0.3-30 > AT0.1-30 > AT0.05-30 >C), zeolites of equivalent porosity prepared by shorter treatments at higher concentration (i.e. AT0.2-5 with respect to AT0.1-30) display smaller mesopores which, at low magnification, appear most prominently along grain boundaries. The scale bars shown in the top row apply to all images in the same column, the symbols on the left correspond to those of the isotherms in Figure S1.

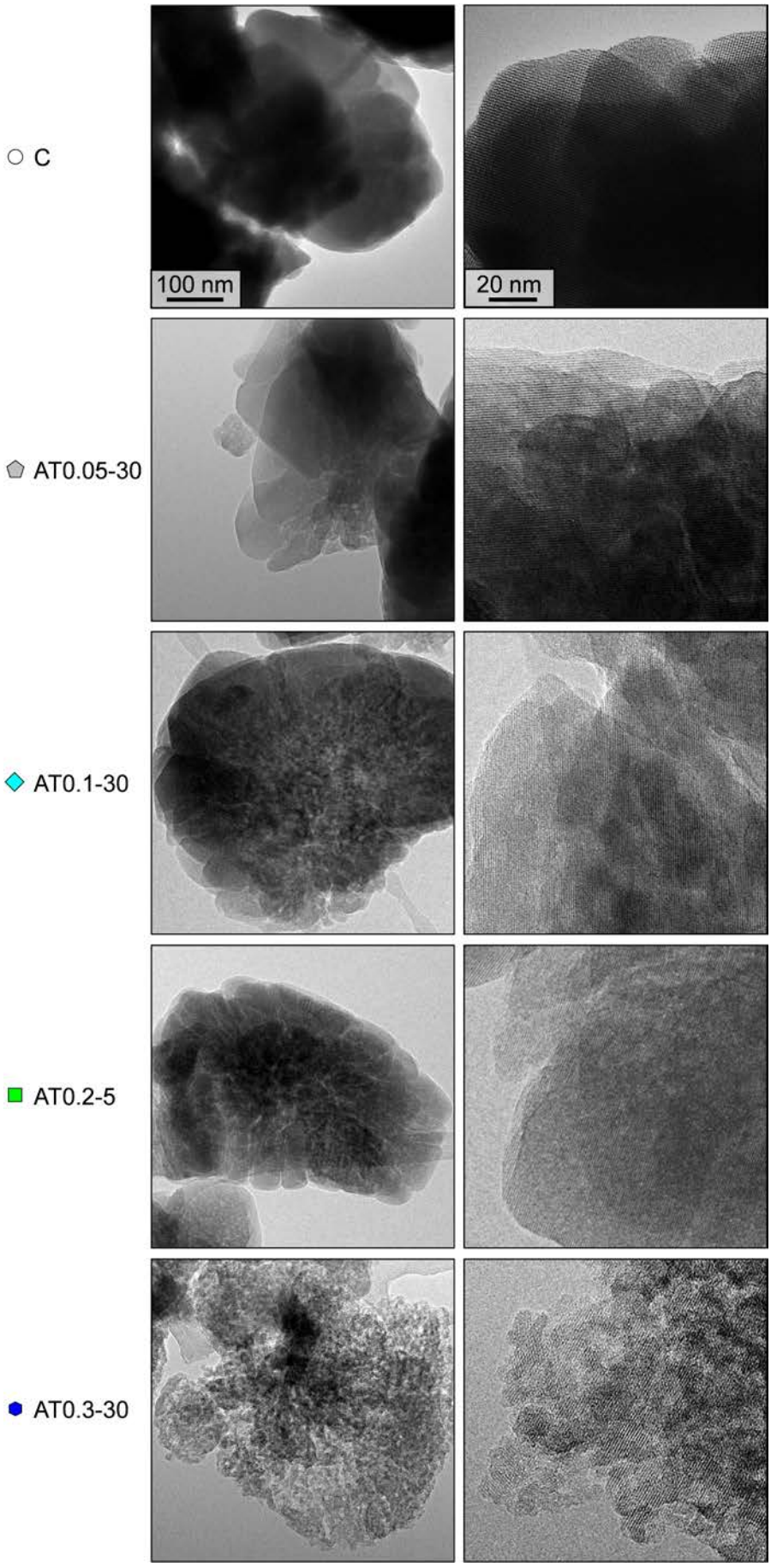
C
100 nm
20 nm
AT0.05-30
AT0.1-30
AT0.2-5
AT0.3-30

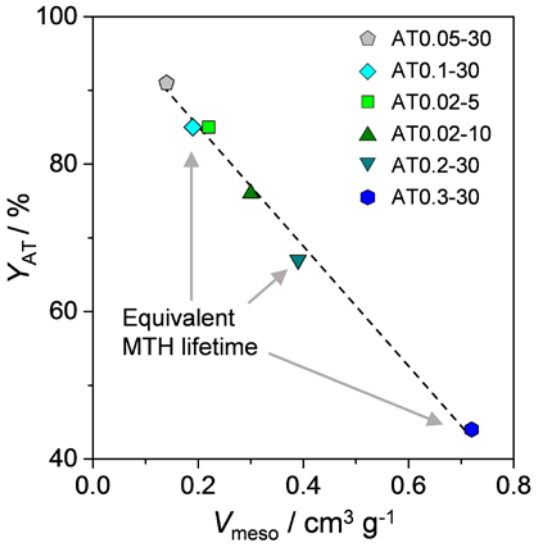

Figure S3. Linear correlation between the yield of the alkaline treatment and the mesopore volume developed.

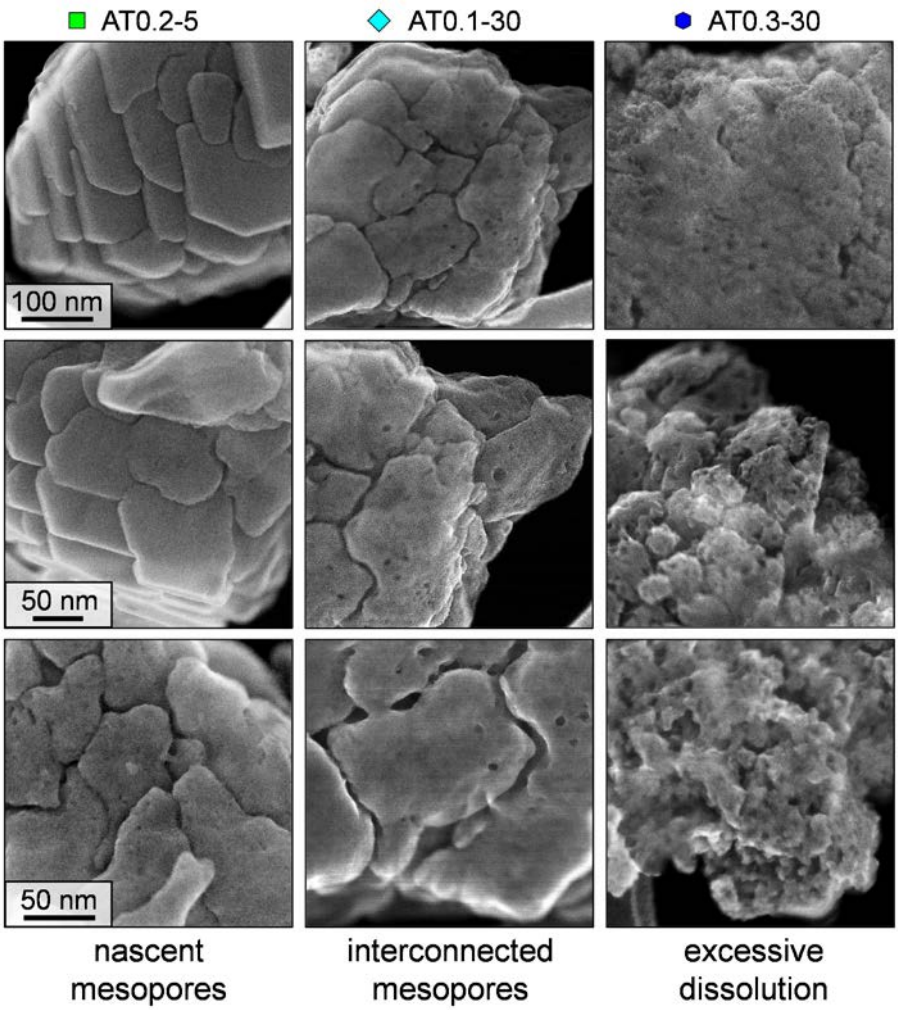

Figure S4. Scanning electron micrographs of further locations of the hierarchical zeolites presented in Figure 3, confirming the distinct modes of mesopore formation. The scale bars shown in the right column apply to all images in the same row, the symbols on the left correspond to those of the isotherms in Figure S1.

Table S1. Methanol-to-hydrocarbons performance of the zeolite catalysts.

Sample	Lifetime[a] h	$S_{C1\text{-}C4\ alkanes}$[b] Cmol%	$S_{C2\text{-}C4\ olefins}$[b] Cmol%	$S_{C5\text{-}C7\ alkanes}$[b] Cmol%	$S_{C6\text{-}C8\ aromatics}$[b] Cmol%
C	16	20	43	20	13
AT0.05-30	29	20	37	27	17
AT0.1-30	55	17	41	25	10
AT0.2-5	20	21	37	24	16
AT0.2-10	26	18	41	25	14
AT0.2-30	58	15	40	26	7
AT0.3-30	53	18	42	28	10

[a] Time for which the conversion of light oxygenates exceeds 95%; [b] average selectivity per cycle (on a carbon mole basis).

Table S2. Lifetimes and their relative intensity of the contributions derived from PALS measurements.

Contribution	Lifetime ps	Intensity -	Lifetime ps	Intensity -]
	C		**AT0.05-30**	
p-Ps[a]	125 (fixed)	0.012 ± 0.024	125 (fixed)	0.006 ± 0.011
e^{+}[b]	792 ± 13	0.687 ± 0.082	792 ± 6	0.785 ± 0.139
$Ps_{micropore}$[c]	2439 ± 1035	0.044 ± 0.040	2840 ± 738	0.011 ± 0.011
$Ps_{defects}$[d]	7363 ± 1068	0.087 ± 0.020	10123 ± 5069	0.028 ± 0.011
$Ps_{mesopore}$[e]	26486 ± 637	0.110 ± 0.002	29436 ± 968	0.068 ± 0.002
Ps_{vacuum}[f]	120965 ± 936	0.126 ± 0.002	129446 ± 655	0.201 ± 0.002
	AT0.1-30		**AT0.2-5**	
p-Ps	125 (fixed)	0.015 ± 0.034	125 (fixed)	0.011 ± 0.023
e^{+}	797 ± 4	0.777 ± 0.297	776 ± 8	0.691 ± 0.177
$Ps_{micropore}$	2126 ± 809	0.008 ± 0.023	2171 ± 955	0.023 ± 0.028
$Ps_{defects}$	5023 ± 383	0.023 ± 0.008	7505 ± 855	0.059 ± 0.016
$Ps_{mesopore}$	25922 ± 1919	0.028 ± 0.002	29486 ± 662	0.108 ± 0.003
Ps_{vacuum}	130243 ± 566	0.203 ± 0.002	131282 ± 705	0.156 ± 0.002
	AT0.2-10		**AT0.2-30**	
p-Ps	125 (fixed)	0.015 ± 0.024	125 (fixed)	0.014 ± 0.016
e^{+}	765 ± 7	0.740 ± 0.149	818 ± 4	0.734 ± 0.016
$Ps_{micropore}$	2594 ± 797	0.019 ± 0.015	2251 ± 783	0.002 ± 0.012
$Ps_{defects}$	8185 ± 1460	0.030 ± 0.006	6337 ± 494	0.019 ± 0.003
$Ps_{mesopore}$	27646 ± 854	0.081 ± 0.001	28352 ± 2123	0.030 ± 0.001
Ps_{vacuum}	131022 ± 687	0.167 ± 0.002	137725 ± 515	0.250 ± 0.002
	AT0.3-30		**AT0.2-30-extrudate**	
p-Ps	125 (fixed)	0.004 ± 0.012	125 (fixed)	0.141 ± 0.205
e^{+}	715 ± 3	0.768 ± 0.078	725 ± 6	0.675 ± 0.330
$Ps_{micropore}$	3433 ± 80	0.027 ± 0.004	2710 ± 269	0.024 ± 0.209
$Ps_{defects}$	-	-	7133 ± 1796	0.011 ± 0.430
$Ps_{mesopore}$	22168 ± 1880	0.029 ± 0.004	42951 ± 2296	0.052 ± 0.002
Ps_{vacuum}	135310 ± 534	0.229 ± 0.000	137060 ± 886	0.162 ± 0.003

Lifetime associated with the annihilation of [a] para-positronium, [b] positron, and ortho-positronium [c] in the zeolite micropores, [d] in structural defects, [e] in the mesopores, and [f] in vacuum.

Table S3. Porous properties of the zeolites determined by N_2 sorption at the start and end (-u) of the MTH cycle.

Sample	V_{micro}[a] $cm^3\ g^{-1}$	V_{meso}[b] $cm^3\ g^{-1}$	S_{meso}[a] $m^2\ g^{-1}$
C	0.17	0.11	78
C-u	0.05	0.10	25
AT0.1-30	0.15	0.19	135
AT0.1-30-u	0.06	0.08	31
AT0.2-5	0.15	0.22	139
AT0.2-5-u	0.05	0.07	39
AT0.3-30	0.09	0.72	376
AT0.3-30-u	0.04	0.35	119

[a] *t*-plot method; [b] $V_{meso} = V_{pore}-V_{micro}$.

References

[1] P. Crivelli, U. Gendotti, A. Rubbia, L. Liszkay, P. Perez, C. Corbelet, *Phys. Rev. A* **2010**, *81*, 52703-1-52703-8.

[2] A. P. Mills, R. J. Wilson, *Phys. Rev. A* **1982**, *26*, 490-500.

[3] C. Pascual-Izarra, A. W. Dong, S. J. Pas, A. J. Hill, B. J. Boyd, C. J. Drummond, *Nucl. Instr. Meth. Phys. A* **2009**, *603*, 456-466.

[4] Complete reference from main manuscript (2j): P. S. Wheatley, P. Chlubná-Eliášová, H. Greer, W. Zhou, V. R. Seymour, D. M. Dawson, S. E. Ashbrook, A. B. Pinar, L. B. McCusker, M. Opanasenko, J. Čejka, R. E. Morris, *Angew. Chem. Int. Ed.* **2014**, doi:10.1002/anie.201407676.

[5] Complete reference from main manuscript (5c): Q. Wang, S. Xu, J. Chen, Y. Wei, J. Li, D. Fan, Z. Yu, Y. Qi, Y. He, S. Xu, C. Yuan, Y. Zhou, J. Wang, M. Zhang, B. Su, Z, Liu, *RSC Adv.* **2014**, *4*, 21479-21491.